In Situ Observations at the Air-Sea Interface by Expendable Air-Deployed Drifters Under Hurricane Michael (2018)

Martha C. Schönau[1] , Theresa Paluszkiewicz[2], Luca R. Centurioni[1] , William A. Komaromi[3] , Hao Jin[4], and James D. Doyle[4]

[1]Scripps Institution of Oceanography, La Jolla, CA, USA, [2]Octopus Ocean Consulting, LLC., Haymarket, VA, USA, [3]NOAA/NWS/OSTI, I.M. Systems Group, Inc., Silver Spring, MD, USA, [4]Naval Research Laboratory, Monterey, CA, USA

Abstract An array of surface drifters deployed ahead of Hurricane Michael measured the surface temperature, pressure, directional wind and wave spectra, and surface currents one day before it made landfall as a Category 5 Hurricane. The drifters, 25–50 km apart, spanned two counter-rotating ocean eddies as Hurricane Michael rapidly intensified. The drifters measured the shift of wave energy between frequency bands in each quadrant of the storm, the response of upper ocean currents, and the resulting cold wake following Michael's passage. Wave energy was greatest in the front quadrants and rapidly decreased in the left-rear quadrant, where wind and wave energy were misaligned, and components of the wave field were aligned with currents. Hurricane Michael's wave field agreed with previous studies of nondirectional wave spectra across multiple tropical cyclones but had some unique characteristics. The analysis demonstrates how co-located surface wind and wave observations can complement existing airborne and satellite observations.

Plain Language Summary Lagrangian drifters were air-deployed ahead of Hurricane Michael and measured the direction and strength of waves and surface wind, sea surface temperature, and sea-level pressure as the storm transited through the central Gulf of Mexico. As Hurricane Michael passed over the drifters, the drifters observed the cyclonic structure of the wind, the shift of wave energy from swell to wind-sea, and the relative mismatch in direction of wind, waves, and ocean currents. In the rear quadrants of the storm, low-frequency waves opposed the wind direction. The drifters, caught in counter-rotating eddies, were ultimately entrained in different sides of the storm. The observations illustrate the importance of a suite of in situ surface observations to complement airborne observing strategies of tropical cyclones.

1. Introduction and Background

After a complex, rapid transit, Hurricane Michael slammed into the Florida Panhandle on 10 October 2018 as a Category 5 hurricane with a minimum pressure of 919 mB, and wind speeds of 72 m s^{-1} (Beven et al., 2019; Le Hénaff et al., 2021; Wadler et al., 2021). Hurricane Michael was the fourth strongest landfalling hurricane recorded in the United States, and the strongest along the Florida Panhandle (National Oceanic and Atmospheric Administration, 2019). The resulting wave and wind fields contributed to a storm surge of 2.7–4.3 m, peaking at Mexico Beach (Beven et al., 2019). During its transit Hurricane Michael experienced moderate vertical shear, but the relative locations of counter-rotating warm- and cold-ring eddies stabilized Michael's symmetry and allowed for strong convection and intensification (Wadler et al., 2021). Assimilation of available temperature and altimetry observations verified the importance of these eddies in forecasting Michael's track and strength (Le Hénaff et al., 2021). Previous studies, however, were limited by the number of in situ surface observations, confounding a full analysis at the air-sea interface, and had no description of Hurricane Michael's wave field.

The air-sea interface under a hurricane is a complex environment, with rapidly changing winds, waves and currents (e.g., Black et al., 2007; D'Asaro et al., 2014). Waves under a hurricane are a mix of swell and wind-sea, highly dependent on the radius, speed, trajectory and quadrant of the storm (e.g., Holthuijsen et al., 2012; Hwang, 2016; Kudryavtsev et al., 2015; Reichl et al., 2014; Young, 2006). The air-sea exchanges of heat, moisture, and momentum that determine a hurricane's strength and intensification rates can depend on wave parameters such as height, direction, and breaking (Bell et al., 2012; Edson et al., 2013; Emanuel, 1995; Fairall et al., 2003; Zhao et al., 2022). Many coupled atmosphere-ocean models parameterize the surface roughness using a wave age dependent Charnock coefficient (e.g., Charnock, 1955; Edson et al., 2013), although there have been

contradictory studies on the nature of this relationship (e.g., Donelan et al., 1993; Fairall et al., 2003; Oost et al., 2002; Smith et al., 1992; Toba et al., 1990; Volkov, 2001).

In the past, hurricane wave field observations have relied on airborne measurements with scanning radar altimeters (Black et al., 2007; PopStefanija et al., 2021; Wright et al., 2001); observations from moored buoys or single autonomous platforms (Collins et al., 2018; Esquivel-Trava et al., 2015; Hu & Chen, 2011; Lenain & Melville, 2014; Tamizi & Young, 2020; Young, 2006); satellite or airborne observations from synthetic aperture radar (Elachi et al., 1977; Holt & Gonzalez, 1986); and subsurface observations with waves derived from Electromagnetic Autonomous Profiling Explorer floats (J. Hsu, 2021; J. Hsu et al., 2018). Several studies have compared hurricane wave observations to wind-driven wave models (e.g., Moon et al., 2004a, 2004b; Moon, Hara, et al., 2004; Fan et al., 2009; Holthuijsen et al., 2012; Montoya et al., 2013; Tamizi et al., 2021; Chen et al., 2022; Zhou et al., 2022), and examined wave growth under hurricanes using self-similar wave growth theory (Hu & Chen, 2011; Hwang, 2016; Kudryavtsev et al., 2015; Tamizi & Young, 2020; Young, 1998, 2003, 2006). The influence of the wave field on the surface drag coefficient continues to be explored (e.g., Black et al., 2007; Davis et al., 2023; Drennan et al., 2003; Moon et al., 2004b), particularly the importance of the angle between wind, waves and surface stress (Holthuijsen et al., 2012; J. Hsu, 2023; J.-Y. Hsu et al., 2019; Moon et al., 2004a; Zhou et al., 2022).

Here we present in situ observations from the sea surface from 10 Lagrangian drifters that sampled sea surface temperature (SST), sea level pressure (SLP), surface wind velocity, currents, and directional wave spectra under Hurricane Michael as it straddled warm and cold-core ocean features just prior to rapidly intensifying. These observations build on past air-deployments of drifters and floats under tropical cyclones (TCs) (Black et al., 2007; D'Asaro et al., 2014; Hormann et al., 2014; Sanabia & Jayne, 2020). Under Hurricane Michael, the suite of drifters was able to resolve the complex surface conditions across all quadrants of the storm. Comparison to previous observations shows that drifters can provide reliable observations to measure surface processes under TCs that are often parameterized by models, complementing existing airborne observations and having broad applications for air-sea research.

2. Data and Methods

Ten satellite-tracked Lagrangian drifters were air-deployed in front of Hurricane Michael's expected path (Figure 1). The array included Surface Velocity Program (SVP) drifters equipped with barometers, Directional Wave Spectra Drifter (DWSD$^{\text{TM}}$) and MiniMet drifters, also called Surface Velocity Program - Barometer Drifters (SVPBWD). All drifters were equipped with a high-quality thermometer to measure SST. Data were relayed to the Lagrangian Drifter Laboratory (LDL) servers in near-real time and subsequently to the Global Telecommunication System (GTS) of the World Weather Watch using Iridium Short Burst Data telemetry. A narrow median filter was applied to all drifter data to remove spurious data points, but no other smoothing or filtering was applied.

SVP drifters follow the near-surface horizontal currents via a ∼6 m holey sock drogue that is centered at 15 m. The National Oceanic and Atmospheric Administration (NOAA) funded Global Drifter Program (Centurioni, Horányi, et al., 2017; Niiler, 2001), the largest component of the Global Surface Drifting Buoy Array (Centurioni et al., 2019), sustains more than 1,250 SVP drifters. When equipped with barometers, the SVP also measures sea level atmospheric pressure (SLP) and is referred to with the acronym Surface Velocity Program drifter with barometer (SVPBD).

The DWSD is a 38 cm diameter undrogued buoy that pairs a performance Global Positioning System (GPS) engine with the LDL developed controller and software algorithm for in situ computation of the directional wave spectrum (Centurioni, Braasch, et al., 2017). The GPS's Doppler shifted satellite signal frequency provides the three velocity components of the buoy and thus of the sea surface motion, assuming that the buoy is a good wave follower. The Fourier transforms of the correlation functions for each pair of the velocity time-series were used to derive the power spectral density, co-spectra and quadrature-spectra parameters, providing the first-5 independent Fourier coefficients: a_0, a_1, b_1, a_2, b_2 (Benoit et al., 1997; Longuet-Higgins et al., 1963). Sampling intervals are at either 30-min or 1-hr, depending on desired setting. The use and accuracy of wave observations using GPS buoys has been established previously by others (Herbers et al., 2012; Thomson, 2012).

The MiniMet drifter (Centurioni, 2018) has been used extensively in early ocean-hurricane interaction programs (D'Asaro et al., 2011; Hormann et al., 2014; Goni et al., 2017) and other scientific studies (Klenz et al., 2022). The
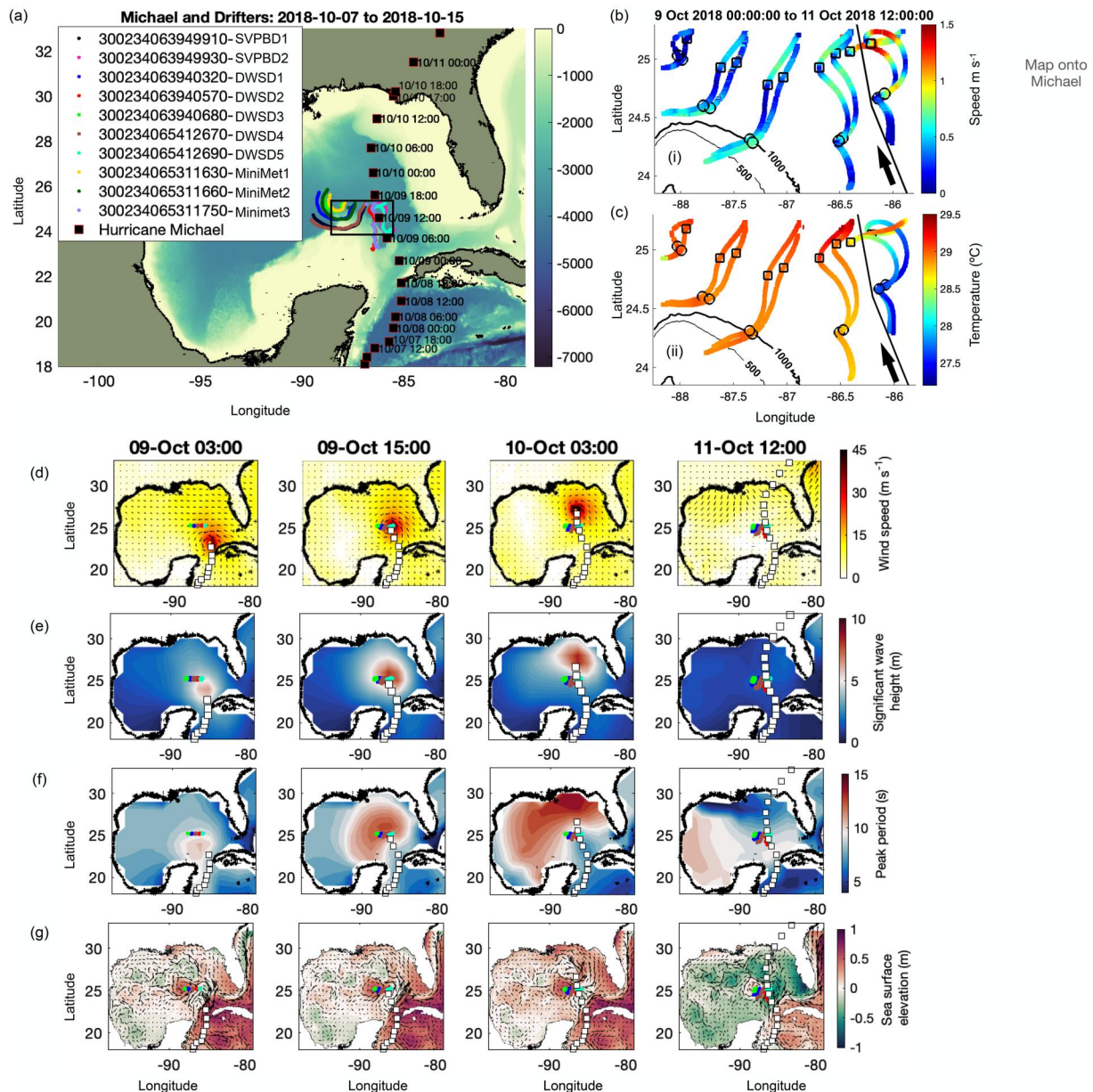
Figure 1. Drifter tracks in relation to Hurricane Michael. (a) Drifters and the National Hurricane Center (NHC) best track from 7 October 2018 to following landfall on 11 October 2018. Drifter tracks are shown from their deployment on 8–15 October 2018. Box shows location of enlarged tracks in (b). The legend provides the drifter identification number and type: Surface Velocity Program drifter with barometer (SVPBD), Directional Wave Spectra Drifter (DWSD), and MiniMet drifter. (b) Drifter tracks colored by velocity as calculated by change in drifter position and (c) Sea Surface Temperature (SST). In (b) and (c), black lines with an arrow indicates the NHC best track; black contours in bottom left are isobaths. Model simulation snapshots: (d) 10-m wind speed and direction from Coupled Ocean/Atmosphere Mesoscale Prediction System for Tropical Cyclones, reduced by 10%, (e) significant wave height from Wave Watch III® (WW3), (f) peak period from WW3, and (g) sea surface elevation (color) and currents (vectors) from the Naval Coastal Ocean Model (NCOM).

MiniMet measures SLP via a barometer, and near-surface wind velocity via a sonic anemometer (up to 60 m s^{-1}; 2% full-scale [FS] accuracy). The wind direction is measured by an internal compass with a directional accuracy of ±2.5°. An on-board quality control algorithm discards the invalid anemometer data that occurs, for example, when the drifter is submerged. Extensive comparisons between MiniMet drifters, 10-m European Center for Medium-Range Weather Forecasts Earth Reanalysis version 5 reanalysis (ERA5) winds, and shipboard observations were made in the North Atlantic (Klenz et al., 2022). The observed MiniMet winds were adjusted to a 10-m height following Klenz et al. (2022) and were in general good agreement with ERA5 away from Hurricane Michael's eye (Figure S1b).

For calculations of wave growth and wave age, 10-m wind was obtained from the Coupled Ocean/Atmosphere Mesoscale Prediction System for Tropical Cyclones (COAMPS-TC). COAMPS-TC (Doyle et al., 2012), developed by the U.S. Naval Research Laboratory and run operationally at Fleet Numerical Oceanography and Meteorology Center, is the Navy's operational forecast model for TCs. COAMPS-TC is a non-hydrostatic, convection-permitting model, featuring a 4-km resolution storm-following nest, and was initialized using a modified Rankine wind vortex that was best fit to Hurricane Michael's wind field, as designated by the National Hurricane Center (NHC) best track. The model simulation wind includes the instantaneous wind, which compared well with the NHC maximum wind, although exceeded the 10-min averaged, 10-m MiniMet winds, especially near Hurricane Michael's core (Figure S1b). The model simulation may have had artificially high instantaneous winds outside the observed inner core, which had a 4-km grid increment in the inner mesh, owing to Hurricane Michael's relatively small radius and its speed. Regression of COAMPS-TC with the 10-min adjusted MiniMet wind during the first 12-hr of observations suggested a scale factor reduction of 10% of the COAMPS-TC strength which was applied to this analysis. COAMPS-TC and MiniMet winds were also compared to 10-m ERA5 winds (1/4°, 1-hr; Figure S1b; Copernicus Climate Change Service (C3S), 2017; Hersbach et al., 2020). ERA5 winds were weaker, and the eye was artificially large caused by the coarser grid spacing.

Bulk wave parameters were available from the University of Hawai'I Global WAVEWATCH III (W3) (1/2°, 1-hr; Cheung, 2010; Tolman, 2009; Figure S1c). These provided background conditions during Hurricane Michael's transit (7–15 October 2018; Figures 1e and 1f) and comparisons to DWSD observations (Figure S1c). The American Seas (AmSeas) Regional Navy Coastal Ocean Model (NCOM; 1/12°, 3-hr; Barron et al., 2006) provided surface currents and dynamic height.

3. Hurricane Michael

Hurricane Michael began as a tropical depression over the western Caribbean Sea, intensifying as it reached the tip of Cuba and moved into the Gulf of Mexico. On the afternoon of 8 October 2018, the stepped frequency microwave radiometer on a 53rd Weather Reconnaissance Squadron (WRS) "Hurricane Hunters" C-130J plane measured windspeed of 20 m s^{-1} (Beven et al., 2019; National Hurricane Center, 1997). During the same flight, 5 DWSDs, 2 SVPBDs, and 3 MiniMet drifters were deployed in a 200 km line array approximately 290–390 km ahead of Hurricane Michael's eye, transecting the storm's projected path (Figure 1a). A drogued SVPBD or a MiniMet drifter was paired with an undrogued DWSD to provide concurrent wave, SLP, wind, and current measurements. The drifters began transmitting data around 23:00 UTC on 8 October 2018. The storm strengthened to an initial peak intensity of a Category 2 hurricane at 9 October 2018 00:00 UTC with winds of 45 m s^{-1} (Beven et al., 2019).

The drifters spanned counter rotating eddies (Le Hénaff et al., 2021; Wadler et al., 2021), an anticyclonic eddy (warm core) to the west and a cyclonic eddy (cold core) to east (Figures 1a, 1b, and 1g). Hurricane Michael transited over the drifters from 9 to 10 October 2018 (Figure 1d). The wind field was slightly asymmetric, with a tight inner core (Figure 1b). On 9 October 2018, the radius of maximum winds (RMW) decreased from 37 km at 00:00:00 to 28 km at 15:00:00, when it encountered the drifters (Figure S1a). Model snapshots show that the greatest wave heights preceded the storm's eye (Figure 1e) with long period swell extending throughout the Gulf of Mexico (Figure 1f). On 9 October, the translational speed was 5–6 m s^{-1} (Figure S1a, NHC Best Track).

3.1. Drifter Observations

At deployment, mean MiniMet 10-m wind speeds ranged from 10 to 15 m s^{-1}, the SLP was 1,006 mB, and SST was 28.5–29.5°C across the array (Figures 2a–2c). The easternmost drifters observed slightly cooler SST, indicating their relative position to the eddies (Figure 1b). Waves preceded the storm's arrival, with significant wave heights ∼4 m and peak period ∼9 s (Figures 2d and 2e). In storm-centered coordinates, the drifters were within 250 km of Hurricane Michael's eye from 9 October 2018 01:30 UTC to 10 October 03:00 UTC (Figure 2, right panels). Hurricane Michael transited over the easternmost drifters (SVPBD2 and DWSD5; Figures 1a and 1b) between 15:00 and 15:30 UTC on 9 October 2018 as a Category 2 storm. At the time, Hurricane Michael's velocity was ∼6 m s^{-1} with a RMW of 28 km (NHC Best Track; Figure S1a).
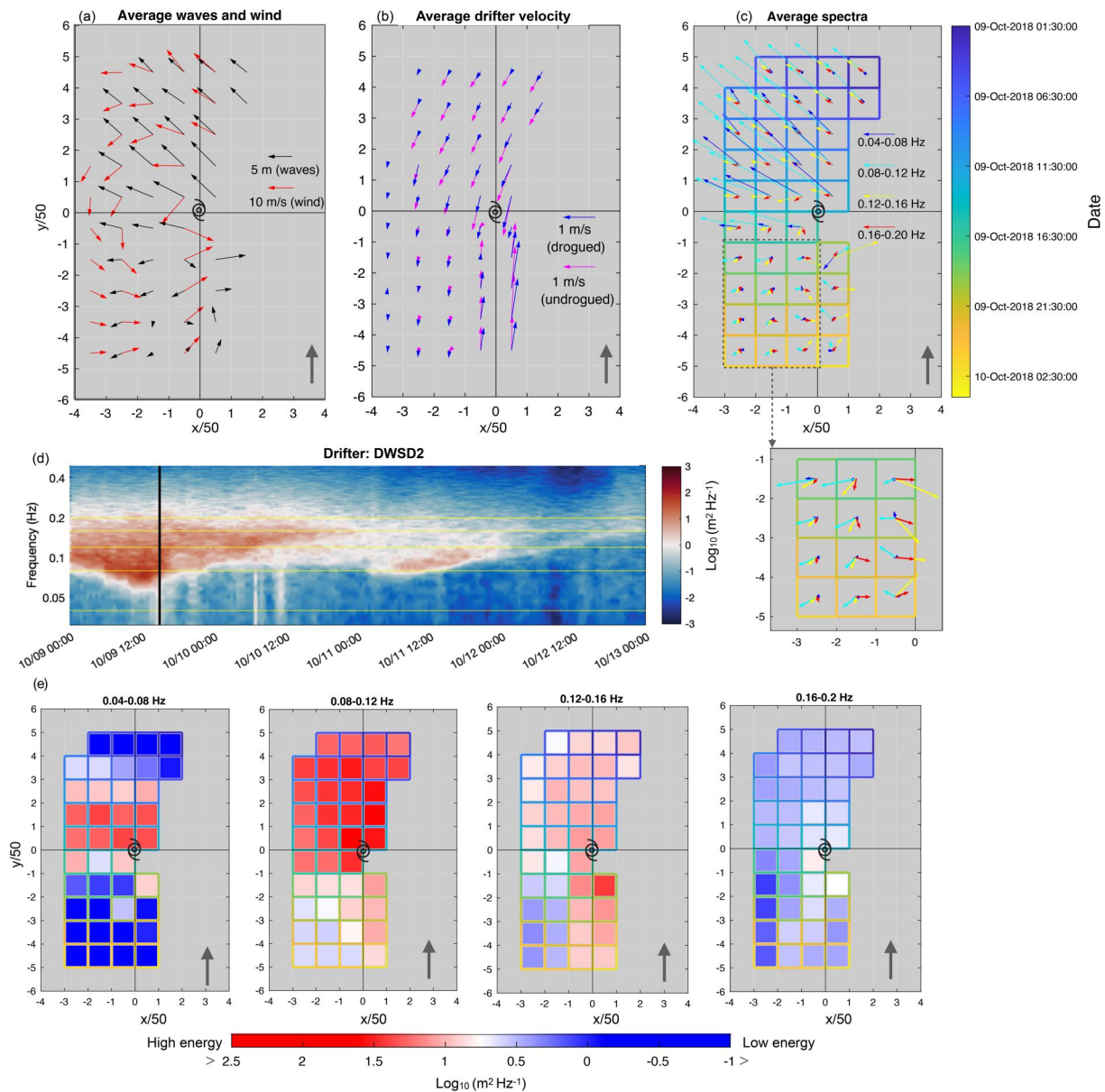
Wind, significant wave height (H_s), and wave peak period (T_p), were greatest in the front quadrants of the storm (Figure 2c). SLP, roughly symmetric around the storm center, had a minimum of 967.6 mB approximately 9.9 km
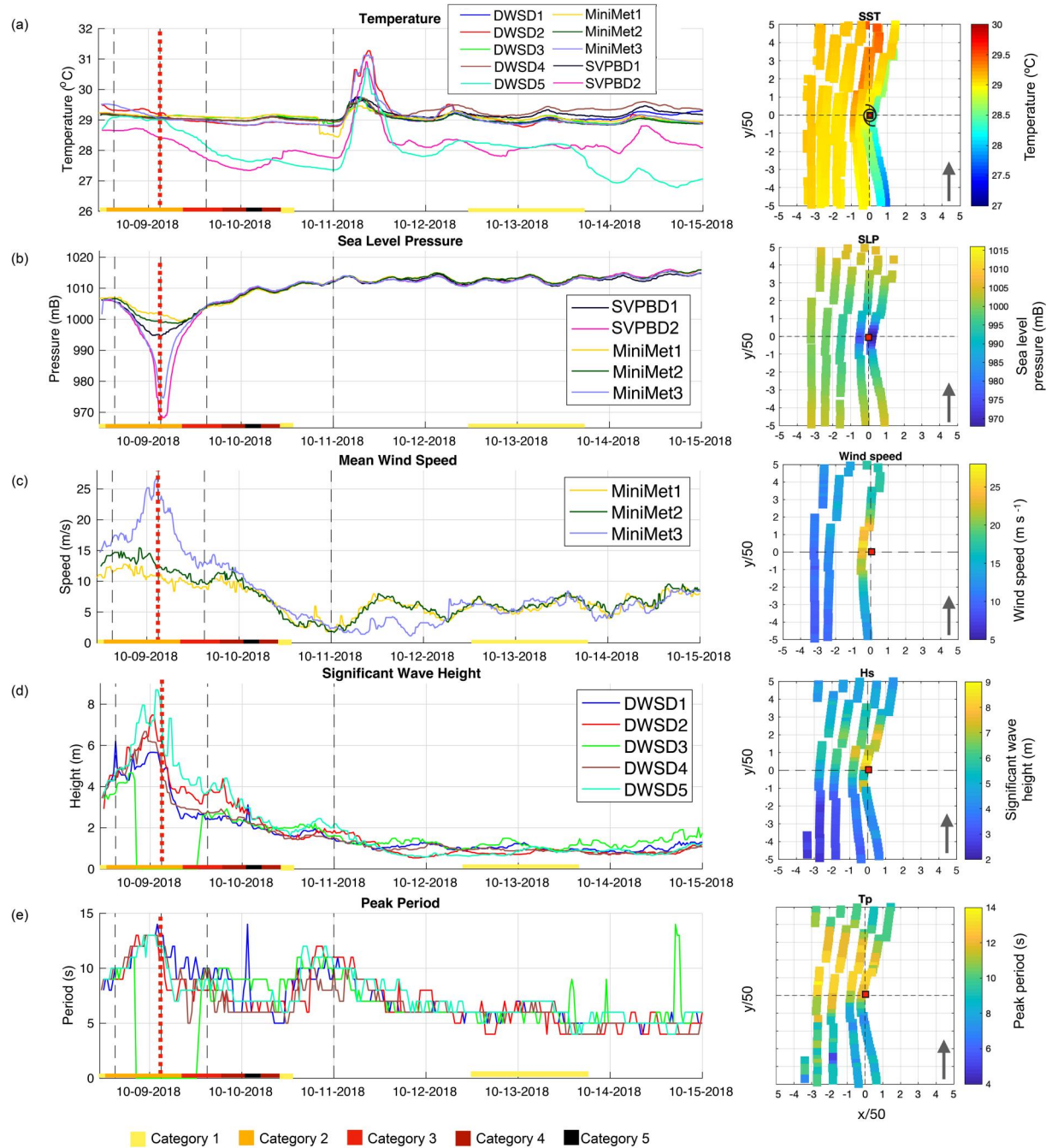
Figure 2. Drifter observations of (a) sea surface temperature, (b) Sea Level Pressure (SLP), (c) mean 10-m wind speed, (d) significant wave height (H_s), and (e) peak period (T_p). H_s and T_p have the same legend. The color bar at the bottom indicates Hurricane Michael's strength on the Saffir-Simpson scale, with the red dotted line at 9 October 2018 15:00 UTC, when Michael's eye transited over the drifters. The black dotted lines are at 9 October 2018 03:00 UTC, 10 October 2018 03:00 UTC, and 11 October 2018 12:00 UTC corresponding to the times of the snapshot in Figure 2. Grid lines fall at 12:00 UTC for each date. The right-hand panels show the variables from each panel transformed with respect to Michael's forward motion (shown by arrow) with axis units normalized by 50 km. The red dot at the center indicates the storm center. Temporally, these observations fall roughly within the first set of black dotted lines in the left-hand panels, over a period of roughly 24-hr (see Figures 3 and 4).

east of the NHC best track (Figure 2b, SVPBD2; 9 October 15:30 UTC). The 10-m mean wind speed peaked at 26.8 m s^{-1}, measured by MiniMet3 at the edge of the NHC Best Track 64 kt (32.9 m s^{-1}) radii. H_s peaked at 8.69 m and T_p at 13 s, roughly 2 hr before the eye's passage (Figures 2d and 2e).

Figure 3. (a) Wind (red) and wave (black) magnitude and direction scaled by the mean wind speed and significant wave height. Quantities were averaged over each of the MiniMet drifters (wind) and Directional Wave Spectra Drifter (DWSD) (waves) observations in 50 km by 50 km bins with respect to Hurricane Michael's forward motion (shown by arrow in bottom right). A small symbol at the center indicates the eye of the storm. Solid black lines separate the storm quadrants. (b) Similar to (a) but for drogued and undrogued speed and direction. (c) Direction and relative wave energy within each frequency bin with respect to Hurricane Michael. The magnitude was averaged in 50 km bins and the direction of peak energy within that bin was rotated with respect to Michael's forward motion. Color around each grid point indicates the average time of the drifter observations, with Hurricane Michael's eye over the drifter array at roughly 9 October 2018 15:00 UTC. The inset below magnifies part of the rear left quadrant by a factor of two. (d) DWSD2 1D wave energy spectrum. Yellow lines mark the frequency bins in (c), and the thick black line at 9 October 2018 15:00 UTC indicates when Hurricane Michael's eye was nearest to the drifter. (e) The mean spectral energy for each of the 0.04–0.08 Hz, 0.08–0.12 Hz, 0.12–0.16 Hz, and 0.16–0.2 Hz bins with respect to Hurricane Michael's forward motion. Color around each grid point indicates the average time of the drifter observations, as indicated in (c), with Hurricane Michael's eye over the drifter array at roughly 9 October 2018 15:00 UTC.

Drogued and undrogued drifters had similar trajectories prior to, during and following Michael's transit (Figure 1b). Drifter velocities to the left of Hurricane Michael's track were 0.2–0.5 m s^{-1} prior to Michael's arrival, with undrogued drifters at greater speeds. Drifters to the right of Hurricane Michael's track had speeds of 1–1.5 m s^{-1} immediately prior to and following Hurricane Michael's passage, with their trajectories changing significantly (Figures 1b and 3b). The alignment of drogued and undrogued drifters nearest to Michael's eye (Figures 1b and 3a), indicates a slab-like advection of the upper 15 m of the ocean (the depth of the drogue). The

two easternmost drifters measured SST cooling of 1°C (Figures 1c and 2a). Following Michael's passage, significant wave height and period rapidly decreased, falling by half within 6 hr (Figures 2d and 2e). The westernmost drifters entered an anticyclonic eddy, and the four eastern drifters proceeded southward with characteristic inertial circles (Figures 1a and 1b).

3.2. Directional Wave and Wind Observations

The magnitude and direction of the wind and waves, averaged in 50 km bins in storm-centered coordinates, changed significantly during Hurricane Michael's passage (Figure 3a), providing a snapshot of the storm structure. The wind was cyclonic around Michael's eye and waves were often at an angle to the wind. In the front quadrants, the dominant wave direction was northwestward (Figure 3a), roughly aligned with the wind in the right-front quadrant and at progressively greater angles to the right of the wind in the left-front quadrant. In the left-rear quadrant, the dominant wave direction was at angles greater than 90° to the wind direction, and at times opposed it.

Averaging the wave spectra in frequency bands, also in 50 km storm-centered coordinates, provides the directional wave energy as a function of frequency under Hurricane Michael (Figure 3c). The frequency, f_p, of the maximum spectral energy was identified within a given band, $S(f_{L-H})$, where f_{L-H} is the frequency range of that band. The direction and energy at f_p were then averaged within that bin. Prior to the storm's arrival, the wave energy was greatest within the 0.08–0.12 Hz frequency band, with energy increasing at lower frequencies (0.04–0.08 Hz) nearer to the storm center (Figures 3c and 3e). At higher frequencies, the direction of peak energy shifted progressively toward the wind direction (Figures 3a and 3c), as expected from stronger wind-wave coupling. In the left-rear quadrant, the decrease in wave energy across all frequency bands corresponded to the dramatic falloff in significant wave height (Figure 2d). In this quadrant, there was rough alignment with currents at middle frequencies (0.8–0.12 Hz) greater than 50 km from the storm center (Figures 3a and 3b). In the right-rear quadrant, the disorganized wave field had eastward and northwestward waves, suggesting a bimodal structure.

3.3. Wave Energy and Wave Age

The 1D variance spectra also shows the shift in spectral energy. For example, the spectral energy of DWSD2 was between 0.08 and 0.2 Hz (Figure 4c). The range broadened and peaked prior to Michael's arrival, then quickly narrowed and decreasing following Michael's passage. (The low-frequency wave energy on 11 October 2018 12:00 UTC was caused by northerly winds over the northern Gulf of Mexico.) Averaging across the drifters in frequency bands and storm-centered coordinates provides the distribution of spectral energy across Hurricane Michael, $\overline{S}(f_{L-H})$ (Figure 3e). The energy was greatest in the front quadrants of the storms, mostly distributed between $\overline{S}(f_{0.08-0.12})$ and $\overline{S}(f_{0.04-0.08})$. $\overline{S}$ was smallest in the left-rear quadrant at frequencies below 0.16 Hz, where wind and waves were most misaligned (Figure 3a). Energy was greatest near the storm's center at frequencies above 0.12 Hz, indicative of wind-sea.

Wave age is a parameter that has been used to analyze the local versus remote response of the wave field, assess wave growth, and parameterize air-sea coupling. The wave age can been alternatively defined as $C_p/|U_{10}|$ (e.g., Donelan, 1990), the phase speed divided by the 10-m wind speed, or as $C_p/|U_{10}|\cos(\theta)$, where θ is the angle difference between the wind and wave directions (e.g., Collins et al., 2018; Grachev & Fairall, 2001; Grachev et al., 2003; C.-E. Hsu et al., 2023; Kudryavtsev et al., 2021). Taking the first definition, wave age for each energy band was calculated across Hurricane Michael (Figure 4a). The phase speed of deep-water waves scales with frequency, $C_p = g/2\pi f_p$, according to the linear dispersion relationship. U_{10}, available from COAMPS-TC, was interpolated to the drifter location. If the wave age is greater (less) than 1.2, then the waves are considered swell (wind-sea) that have been remotely (locally) generated (Donelan, 1990). Using this definition, swell conditions existed in the lowest frequency band (0.04–0.08 Hz) furthest from the storm center, with wind-sea dominating nearer to the center of the storm (Figure 4a). At frequencies greater than 0.12 Hz wind-sea conditions existed across the storm as expected.

These observations can be compared to fetch-limited wave growth under TCs by plotting the non-dimensional energy, $\varepsilon = g^2 E_{tot}/U_{10}^4$, versus the inverse wave age, $\nu = f_p U_{10}/g$ scaled by 2π (Young, 2006). Here g is the Earth's gravitational constant and $E_{tot} = (H_s/4)^2$ is the integrated wave energy (Figure 4b). This comparison can be done either with DWSD-MiniMet pairs (e.g., DWS1-MiniMet2 and DWS2-MiniMet3) or using COAMPS-TC
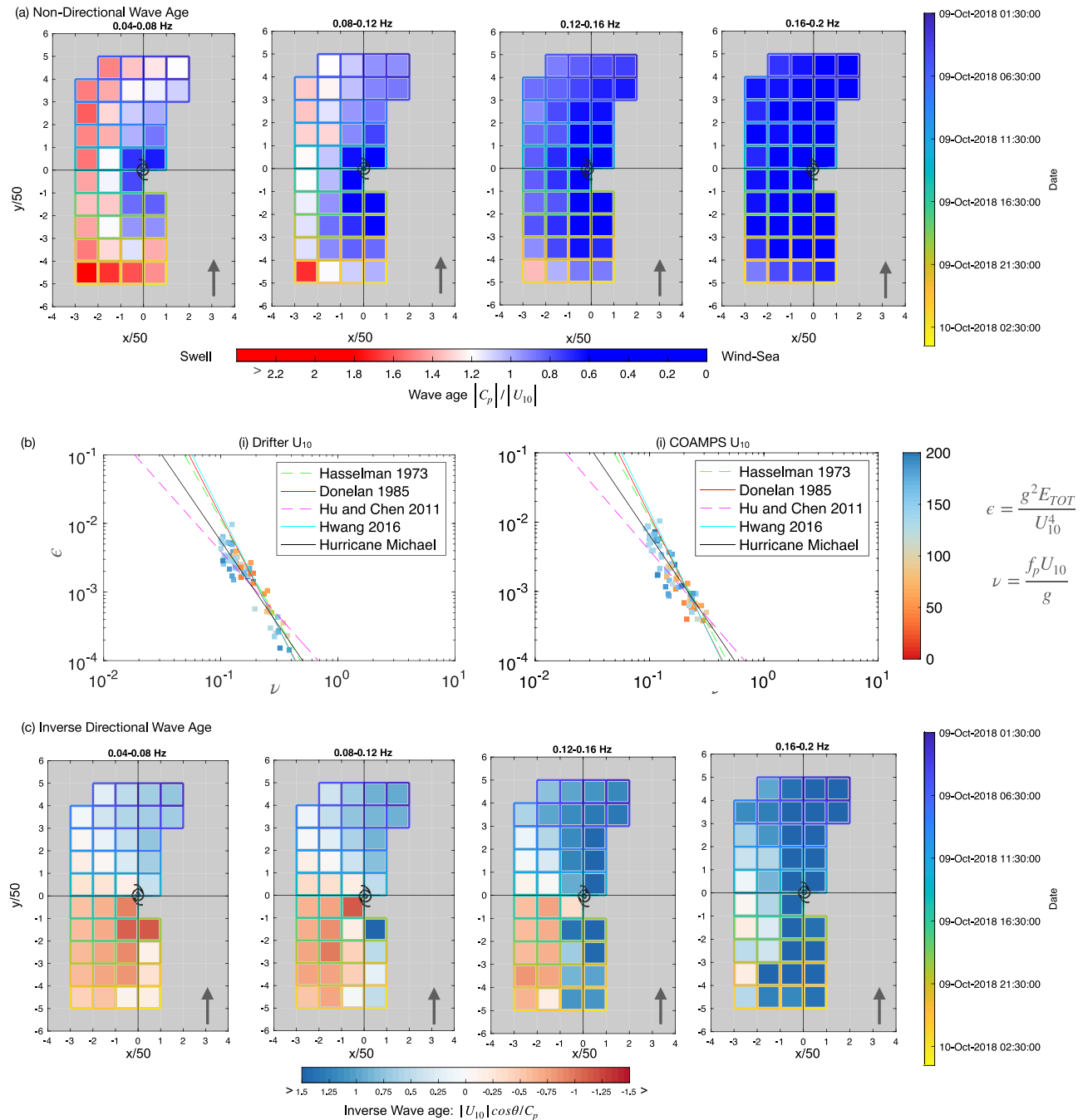
Figure 4. (a) Wave age by frequency band averaged over the Directional Wave Spectra Drifter (DWSD) observations, translated with respect to Hurricane Michael's forward motion and averaged in a 50 km by 50 km bin. (b) Nondimensionalized wave energy versus nondimensionalized inverse wave age (normalized by 2π) compared to other observational results from tropical cyclones and fetch-limited cases, with the wind from either the (i) drifter U_{10} and (ii) Coupled Ocean/Atmosphere Mesoscale Prediction System for Tropical Cyclones (COAMPS-TC) U_{10} (right). For (i), only data points where DWSD and MiniMet drifters were in the same 50 km^2 box were included. (c) Inverse "directional" wave age. As in Figure 3c, color around each grid point in (a) and (c) indicates the average time of the drifter observations.

winds. The results were similar between the two and agree with previous observational studies using a moored platforms under TCs and those of fetch-limited conditions with unidirectional winds (Donelan et al., 1985; Hasselmann et al., 1973; Hu & Chen, 2011; Hwang, 2016; Young, 2006). Using ERA5 instead of COAMPS-TC (not shown) led to poor agreement, emphasizing the importance of a wind field that resolves the maximum wind speeds at the storm center.

The previous wave age definition doesn't incorporate direction and may not completely account for air-wave-ocean dynamics that determine the drag coefficient (Zhou et al., 2022). An inverse "directional" wave age, $|U_{10}|\cos(\theta)/C_p$, as referenced above, can be used to examine the wind-wave direction mismatch, using the inverse to avoid the singularity at $\theta = 90°$. In the left-rear quadrant, the dominant wave direction opposed the wind within the 0.04–0.16 Hz frequency bands (Figure 4c). Comparing Figures 3d and 4c, wave energy was low in many of the locations where the directional wave age was "negative," such as in the far left-rear quadrant. However, at times dominant wave energy opposed the wind, particularly directly to the left of the eye.

4. Discussion and Conclusion

Drifters observed the evolution of SLP, SST, waves, winds, and currents under Hurricane Michael, spanning warm- and cold-core eddies. The observations were consistent with modeled winds, wave heights, and NHC best track information and were able to resolve wind, wave, and current magnitudes and directionality. Of particular interest is the rear-left quadrant where the misalignment between wind and wave directions was greatest, and wave-current interaction could have been an influencing factor in wave height.

These observations confirm what several other observational and numerical studies have found about TC wave fields (e.g., Black et al., 2007; Holthuijsen et al., 2012; Hwang & Walsh, 2018; Young, 2006): in the right-front quadrant extended fetch occurs and there is relative alignment of wind and waves, and in the rear quadrants the waves were at greater direction to the wind showing greater misalignment. Several studies have found that TC wave fields are dependent on the storm transit speed, RMW, and distance from the eye (Kudryavtsev et al., 2015; Moon et al., 2003, 2004a; Reichl et al., 2014; Tamizi et al., 2021). Hurricane Michael had a radius, R, of roughly 30 km, making the analysis here to 250 km ($\sim 8R$) reasonable. The storm transited at an average speed (5–8 m/s), with a ratio of maximum winds to speed of about 0.1–0.15, putting it within the limits of trapped and enhanced waves in the right front quadrant (Kudryavtsev et al., 2015) and providing energy for an asymmetric wave field, as was observed. The drifter observations matched the non-dimensional empirical growth relationship when using both the observed MiniMet and COAMPS-TC winds (Figure 4c). However, some of the ocean interactions with Hurricane Michael were unique. In Hurricane Michael, waves had greater alignment with wind in the front quadrants and were at greater angles to the wind in the rear-left quadrant when compared to composites across multiple TCs (Esquivel-Trava et al., 2015; Hu & Chen, 2011; Tamizi & Young, 2020). There was some evidence of bimodal spectra (Figure 3c), as has been found by other studies (Collins et al., 2018; Holthuijsen et al., 2012; Hu & Chen, 2011; Hwang & Walsh, 2018).

Drogued drifters were advected according to the upper-ocean dynamic response (from the surface to 15 m depth). Undrogued drifters moved faster than drogued drifters preceding the storm likely because they are more vulnerable to local winds and Stokes drift. The drifters aligned in Hurricane Michael's immediate wake (Figure 3b), suggesting that upper-ocean vertical shear was small, and the upper ocean moved as a slab. The dramatic shift in direction directly under the storm was consistent with other studies (Chang et al., 2013, 2016; Ginis & Sutyrin, 1995). Observations of uniform currents to a depth of 50 m have previously been made in a hurricane's wake (J. Hsu et al., 2017), but there were not sufficient subsurface measurements under Hurricane Michael to complete a full upper-ocean analysis.

The drifter trajectories were not in the direction of either the wind or waves in the front quadrants of the storm (Figures 1b, 3a, and 3b). Alignment of the currents and waves (Figures 3a and 3b) in the left-rear quadrant could have created a wave-current interaction favorable to a reduction in H_s (Fan et al., 2009; Hegermiller et al., 2019). This may have contributing to the reduction of wave energy measured in this quadrant (Figures 2d and 3e).

The relative wind and wave directions as a function of frequency band were illustrated by the inverse "directional" wave age. Here the $\cos(\theta)$ term, which should be used with care when determining swell and wind-sea (e.g., Högström et al., 2011; Smedman et al., 2009), was used to emphasize the angle mismatch. A plot of θ had a similar pattern (e.g., Figure A1 of Holthuijsen et al., 2012), with the angle exceeding 100° in much of the left-rear quadrant at frequencies below 0.16 Hz. The direction and magnitude of the wind and waves are critical to surface roughness and momentum transfer. In the case of the rear-quadrant, the misalignment could have significant impacts on the drag coefficient (Chen et al., 2022; Drennan et al., 1999; Grachev et al., 2003; Holthuijsen et al., 2012; J. Hsu, 2023; J. Hsu et al., 2017; J.-Y. Hsu et al., 2019; Moon et al., 2004a; Reichl et al., 2014; Zhou et al., 2022).

Under Hurricane Michael, the 30–60 km instrument spacing resolved the wave field, but optimal spacing depends on the storm parameters (e.g., radii, transit speed). The bin averaging of 50 km used in this analysis, was based on drifter sampling, providing roughly 5–6 observations in each bin and full coverage across the storm. Finer averaging (e.g., 25 km) did not significantly alter results and led to gaps in the analysis, whereas greater bin size led to averaging over dissimilar storm structure. Drifters were deployed in a single line with observations taken over a 24-hr period. In the future, deployment of two drifter lines would better assess the storm's temporal evolution.

The observations under Hurricane Michael show the capability of air-deployed Lagrangian drifters to obtain a suite of in situ measurements at the air-sea interface under TCs. The drifters provided direct measures of directional surface wind, wave, and currents across multiple quadrants of the storm, variables that often need to be extrapolated or parameterized instead of measured directly (e.g., J. Hsu et al., 2018; Zhang & Uhlhorn, 2012; Zhou et al., 2022). The relative low-cost, and ease of the drifter deployment provides an additional research tool to complement existing airborne and satellite observational strategies.

Data Availability Statement

Hurricane Michael drifter data is available from Centurioni et al. (2022a, 2022b).

The Hurricane Michael COAMPS-TC simulation is available from Schönau et al. (2024).

ERA5 reanalysis data on single levels (1950-present) is available from the Copernicus climate service (https://cds.climate.copernicus.eu/) at https://cds.climate.copernicus.eu/cdsapp#!/dataset/reanalysis-era5-single-levels?tab=overview.

WW3 Global model output is available from the Pacific Island Ocean Observing System (PACIOOS; https://pae-paha.pacioos.hawaii.edu/erddap/) at https://pae-paha.pacioos.hawaii.edu/erddap/griddap/ww3_global_lon180.html.

Regional AmSeas NCOM is available from the National Center for Environmental Information (https://www.ncei.noaa.gov/erddap/) for surface velocities at https://www.ncei.noaa.gov/erddap/griddap/NCOM_amseas_latest3d.html and surface elevations at https://www.ncei.noaa.gov/erddap/griddap/NCOM_amseas_latest2d.html.

National Hurricane Center (NHC) archives observations from the 53rd WRS (https://www.nhc.noaa.gov/recon.php) at https://www.nhc.noaa.gov/archive/recon/2018/REPNT2/, and NHC Best Track information for Hurricane Michael is available from the Hurricane Databases (HURDAT; https://www.nhc.noaa.gov/data/#hurdat) at https://www.nhc.noaa.gov/data/hurdat/hurdat2-1851-2021-100522.txt.

References

Barron, C. N., Kara, A. B., Martin, P. J., Rhodes, R. C., & Smedstad, L. F. (2006). Formulation, implementation and examination of vertical coordinate choices in the Global Navy Coastal Ocean Model (NCOM). *Ocean Modelling*, *11*(3–4), 347–375. https://doi.org/10.1016/j.ocemod.2005.01.004

Bell, M. M., Montgomery, M. T., & Emanuel, K. A. (2012). Air–sea enthalpy and momentum exchange at major hurricane wind speeds observed during CBLAST. *Journal of the Atmospheric Sciences*, *69*(11), 3197–3222. https://doi.org/10.1175/JAS-D-11-0276.1

Benoit, M., Frigaard, P., & Schäffer, H. A. (1997). Analysing multidirectional wave spectra. In E. Mansard (Ed.), *Proceedings of the 27th IAHR Congress, San Francisco, 10–15 August 1997: IAHR seminar: Multidirectional waves and their interaction with structures*. Canadian Government Publishing.

Beven, J., Berg, R., & Hagen, A. (2019). *Tropical cyclone report: Hurricane Michael*. NOAA Report AL-142018. National Hurricane Center.

Black, P. G., D'Asaro, E. A., Drennan, W. M., French, J. R., Niiler, P. P., Sanford, T. B., et al. (2007). Air–sea exchange in hurricanes: Synthesis of observations from the coupled boundary layer air–sea transfer experiment. *Bulletin of the American Meteorological Society*, *88*(3), 357–374. https://doi.org/10.1175/BAMS-88-3-357

Centurioni, L. R. (2018). Drifter technology and impacts for sea surface temperature, sea-level pressure, and ocean circulation studies. In R. Venkatesan, A. Tandon, E. D'Asaro, & M. A. Atmanand (Eds.), *Observing the oceans in real time* (pp. 37–57). Springer International Publishing.

Centurioni, L. R., Braasch, L., Di Lauro, E., Contestabile, P., De Leo, F., Casotti, R., et al. (2017). A new strategic wave measurement station off Naples port main breakwater. *Coastal Engineering Proceedings*, *1*(35), waves.36. https://doi.org/10.9753/op.v35.waves.36

Centurioni, L. R., Horányi, A., Cardinali, C., Charpentier, E., & Lumpkin, R. (2017). A global ocean observing system for measuring sea level atmospheric pressure: Effects and impacts on numerical weather prediction. *Bulletin of the American Meteorological Society*, *98*(2), 231–238. https://doi.org/10.1175/BAMS-D-15-00080.1

Centurioni, L. R., Paluszkiewicz, T., & Schönau, M. C. (2022a). Lagrangian Drifter Laboratory at Scripps Institution of Oceanography Hurricane Michael (2018) drifter data [Dataset]. Lagrangian Drifter Laboratory, Scripps Institution of Oceanography. https://doi.org/10.57969/S94W2D

Centurioni, L. R., Paluszkiewicz, T., & Schönau, M. C. (2022b). Lagrangian Drifter Laboratory at Scripps Institution of Oceanography Hurricane Michael (2018) first-five wave data [Dataset]. Lagrangian Drifter Laboratory, Scripps Institution of Oceanography. https://doi.org/10.57969/S9159W

Centurioni, L. R., Turton, J., Lumpkin, R., Braasch, L., Brassington, G., Chao, Y., et al. (2019). Global in situ observations of essential climate and ocean variables at the air–sea interface. *Frontiers in Marine Science*, 6, 419. https://doi.org/10.3389/fmars.2019.00419

Chang, Y.-C., Chen, G.-Y., Tseng, R.-S., Centurioni, L. R., & Chu, P. C. (2013). Observed near-surface flows under all tropical cyclone intensity levels using drifters in the northwestern Pacific. *Journal of Geophysical Research: Oceans*, 118(5), 2367–2377. https://doi.org/10.1002/jgrc.20187

Chang, Y.-C., Tseng, R.-S., Chu, P. C., Chen, J.-M., & Centurioni, L. R. (2016). Observed strong currents under global tropical cyclones. *Journal of Marine Systems*, 159, 33–40. https://doi.org/10.1016/j.jmarsys.2016.03.001

Charnock, H. (1955). Wind stress on a water surface. *Quarterly Journal of the Royal Meteorological Society*, 81(350), 639–640. https://doi.org/10.1002/qj.49708135027

Chen, S., Qiao, F., Zhang, J. A., Xue, Y., Ma, H., & Chen, S. (2022). Observed drag coefficient asymmetry in a tropical cyclone. *Journal of Geophysical Research: Oceans*, 127(9), e2021JC018360. https://doi.org/10.1029/2021JC018360

Cheung, K. F. (2010). WaveWatch III (WW3) global wave model. [07OCT2018 to 15OCT2018] Distributed by the Pacific Islands Ocean Observing System (PacIOOS). Updated 2021. Retrieved from http://pacioos.org/metadata/ww3_global/WaveWatch_III_Global_Wave_Model_best.ncd.html

Collins, C. O., Potter, H., Lund, B., Tamura, H., & Graber, H. C. (2018). Directional wave spectra observed during intense tropical cyclones. *Journal of Geophysical Research: Oceans*, 123(2), 773–793. https://doi.org/10.1002/2017JC012943

Copernicus Climate Change Service (C3S). (2017). *ERA5: Fifth generation of ECMWF atmospheric reanalyses of the global climate*. Copernicus Climate Change Service Climate Data Store (CDS). Retrieved from https://cds.climate.copernicus.eu/cdsapp#!/home

D'Asaro, E. A., Black, P., Centurioni, L., Harr, P., Jayne, S., Lin, I.-I., et al. (2011). Typhoon-ocean interaction in the western North Pacific: Part 1. *Oceanography*, 24(4), 24–31. https://doi.org/10.5670/oceanog.2011.91

D'Asaro, E. A., Black, P. G., Centurioni, L. R., Chang, Y., Chen, S. S., Foster, R. C., et al. (2014). Impact of typhoons on the ocean in the Pacific. *Bulletin of the American Meteorological Society*, 95(9), 1405–1418. https://doi.org/10.1175/BAMS-D-12-00104.1

Davis, J. R., Thomson, J., Houghton, I. A., Doyle, J. D., Komaromi, W. A., Fairall, C. W., et al. (2023). Saturation of ocean surface wave slopes observed during hurricanes. *Geophysical Research Letters*, 50(16), e2023GL104139. https://doi.org/10.1029/2023GL104139

Donelan, M. A. (1990). Air–sea interaction. In B. LéMehauté & D. Hanes (Eds.), *The sea* (Vol. 9A, pp. 239–292). Wiley.

Donelan, M. A., Dobson, F. W., Smith, S. D., & Anderson, R. J. (1993). On the dependence of sea surface roughness on wave development. *Journal of Physical Oceanography*, 23(9), 2143–2149. https://doi.org/10.1175/1520-0485(1993)023<2143:OTDOSS>2.0.CO;2

Donelan, M. A., Hamilton, J., & Hui, W. (1985). Directional spectra of wind-generated ocean waves. *Philosophical Transactions of the Royal Society of London. Series A, Mathematical and Physical Sciences*, 315(1534), 509–562. https://doi.org/10.1098/rsta.1985.0054

Doyle, J. D., Hodur, R. M., Chen, S., Jin, Y., Moskaitis, J. R., Wang, S., et al. (2014). Tropical cyclone prediction using COAMPS-TC. *Oceanography*, 27(3), 104–115. https://doi.org/10.5670/oceanog.2014.72

Doyle, J. D., Jin, Y., Hodur, R. M., Chen, S., Jin, H., Moskaitis, J., et al. (2012). Real-time tropical cyclone prediction using COAMPS-TC. In *Advances in geophysics* (Vol. 28, pp. 15–28). Academic Press. https://doi.org/10.1142/9789814405683_0002

Drennan, W. M., Graber, H. C., & Donelan, M. A. (1999). Evidence for the effects of swell and unsteady winds on marine wind stress. *Journal of Physical Oceanography*, 29(8), 1853–1864. https://doi.org/10.1175/1520-0485(1999)029<1853:EFTEOS>2.0.CO;2

Drennan, W. M., Graber, H. C., Hauser, D., & Quentin, C. (2003). On the wave age dependence of wind stress over pure wind seas. *Journal of Geophysical Research*, 108(C3), 8062. https://doi.org/10.1029/2000JC000715

Edson, J. B., Jampana, V., Weller, R. A., Bigorre, S. P., Plueddemann, A. J., Fairall, C. W., et al. (2013). On the exchange of momentum over the open ocean. *Journal of Physical Oceanography*, 43(8), 1589–1610. https://doi.org/10.1175/JPO-D-12-0173.1

Elachi, C., Thompson, T. W., & King, D. (1977). Ocean wave patterns under Hurricane Gloria: Observations with an airborne synthetic aperture radar. *Science*, 198(4317), 609–610. https://doi.org/10.1126/science.198.4317.609

Emanuel, K. A. (1995). Sensitivity of tropical cyclones to surface exchange coefficients and a revised steady-state model incorporating eye dynamics. *Journal of the Atmospheric Sciences*, 52(22), 3969–3976. https://doi.org/10.1175/1520-0469(1995)052<3969:SOTCTS>2.0.CO;2

Esquivel-Trava, B., Ocampo-Torres, F. J., & Osuna, P. (2015). Spatial structure of directional wave spectra in hurricanes. *Ocean Dynamics*, 65(1), 65–76. https://doi.org/10.1007/s10236-014-0791-9

Fairall, C. W., Bradley, E. F., Hare, J. E., Grachev, A. A., & Edson, J. B. (2003). Bulk parameterization of air–sea fluxes: Updates and verification for the COARE algorithm. *Journal of Climate*, 16(4), 571–591. https://doi.org/10.1175/1520-0442(2003)016<0571:BPOASF>2.0.CO;2

Fan, Y., Ginis, I., Hara, T., Wright, C. W., & Walsh, E. J. (2009). Numerical simulations and observations of surface wave fields under an extreme tropical cyclone. *Journal of Physical Oceanography*, 39(9), 2097–2116. https://doi.org/10.1175/2009JPO4224.1

Ginis, I., & Sutyrin, G. (1995). Hurricane-generated depth-averaged currents and sea surface elevation. *Journal of Physical Oceanography*, 25(6), 1218–1242. https://doi.org/10.1175/1520-0485(1995)025<1218:HGDACA>2.0.CO;2

Goni, G. J., Todd, R. E., Jayne, S. R., Halliwell, G., Glenn, S., Dong, J., et al. (2017). Autonomous and Lagrangian ocean observations for Atlantic tropical cyclone studies and forecasts. *Oceanography*, 30(2), 92–103. https://doi.org/10.5670/oceanog.2017.227

Grachev, A. A., & Fairall, C. W. (2001). Upward momentum transfer in the marine boundary layer. *Journal of Physical Oceanography*, 31(7), 1698–1711. https://doi.org/10.1175/1520-0485(2001)031<1698:UMTITM>2.0.CO;2

Grachev, A. A., Fairall, C. W., Hare, J. E., Edson, J. B., & Miller, S. D. (2003). Wind stress vector over ocean waves. *Journal of Physical Oceanography*, 33(11), 2408–2429. https://doi.org/10.1175/1520-0485(2003)033<2408:WSVOOW>2.0.CO;2

Hasselmann, K., Barnett, T., Bouws, E., Carlson, H., Cartwright, D., Enke, K., et al. (1973). Measurements of wind-wave growth and swell decay during the joint North Sea wave project (JONSWAP). *Ergänzungsheft zur Deutschen Hydrographischen Zeitschrift, Reihe A* (8), 12, 1–95.

Hegermiller, C. A., Warner, J. C., Olabarrieta, M., & Sherwood, C. R. (2019). Wave–current interaction between Hurricane Matthew wave fields and the Gulf Stream. *Journal of Physical Oceanography*, 49(11), 2883–2900. https://doi.org/10.1175/JPO-D-19-0124.1

Herbers, T. H. C., Jessen, P. F., Janssen, T. T., Colbert, D. B., & MacMahan, J. H. (2012). Observing ocean surface waves with GPS-tracked buoys. *Journal of Atmospheric Technology*, 29(7), 944–959. https://doi.org/10.1175/JTECH-D-11-00128.1

Hersbach, H., Bell, B., Berrisford, P., Hirahara, S., Horányi, A., Muñoz-Sabater, J., et al. (2020). The ERA5 global reanalysis. *Quarterly Journal Royal Meteorological Society*, 146(730), 1999–2049. https://doi.org/10.1002/qj.3803

Högström, U., Smedman, A., Semedo, A., & Rutgersson, A. (2011). Comments on "A global climatology of wind–wave interaction". *Journal of Physical Oceanography*, 41(9), 1811–1813. https://doi.org/10.1175/JPO-D-10-05015.1

Holt, B., & Gonzalez, F. I. (1986). SIR-B observations of dominant ocean waves near Hurricane Josephine. *Journal of Geophysical Research*, 91(C7), 8595–8598. https://doi.org/10.1029/JC091iC07p08595

Holthuijsen, L. H., Powell, M. D., & Pietrzak, J. D. (2012). Wind and waves in extreme hurricanes. *Journal of Geophysical Research*, 117(C9), C09003. https://doi.org/10.1029/2012JC007983

Hormann, V., Centurioni, L. R., Rainville, L., Lee, C. M., & Braasch, L. J. (2014). Response of upper ocean currents to Typhoon Fanapi. *Geophysical Research Letters*, *41*(11), 3995–4003. https://doi.org/10.1002/2014GL060317

Hsu, C.-E., Hegermiller, C. A., Warner, J. C., & Olabarrieta, M. (2023). Ocean surface gravity wave evolution during three along-shelf propagating tropical cyclones: Model's performance of wind-sea and swell. *Journal of Marine Science and Engineering*, *11*(6), 1152. https://doi.org/10.3390/jmse11061152

Hsu, J. (2021). Observing surface wave directional spectra under Typhoon Megi (2010) using subsurface EM-APEX floats. *Journal of Atmospheric and Oceanic Technology*, *38*(11), 1949–1966. https://doi.org/10.1175/JTECH-D-20-0210.1

Hsu, J. (2023). Effect of wave directions on orientation and magnitude of surface wind stress under Typhoon Megi (2010). *Journal of Physical Oceanography*, *53*(7), 1767–1785. https://doi.org/10.1175/JPO-D-22-0193.1

Hsu, J., Lien, R., D'Asaro, E. A., & Sanford, T. B. (2017). Estimates of surface wind stress and drag coefficients in Typhoon Megi. *Journal of Physical Oceanography*, *47*(3), 545–565. https://doi.org/10.1175/JPO-D-16-0069.1

Hsu, J., Lien, R., D'Asaro, E. A., & Sanford, T. B. (2018). Estimates of surface waves using subsurface EM-APEX floats under Typhoon Fanapi 2010. *Journal of Atmospheric and Oceanic Technology*, *35*(5), 1053–1075. https://doi.org/10.1175/JTECH-D-17-0121.1

Hsu, J.-Y., Lien, R.-C., D'Asaro, E. A., & Sanford, T. B. (2019). Scaling of drag coefficients under five tropical cyclones. *Geophysical Research Letters*, *46*(6), 3349–3358. https://doi.org/10.1029/2018GL081574

Hu, K., & Chen, Q. (2011). Directional spectra of hurricane-generated waves in the Gulf of Mexico. *Geophysical Research Letters*, *38*(19), L19608. https://doi.org/10.1029/2011GL049145

Hwang, P. A. (2016). Fetch- and duration-limited nature of surface wave growth inside tropical cyclones: With applications to air–sea exchange and remote sensing. *Journal of Physical Oceanography*, *46*(1), 41–56. https://doi.org/10.1175/JPO-D-15-0173.1

Hwang, P. A., & Walsh, E. J. (2018). Propagation directions of ocean surface waves inside tropical cyclones. *Journal of Physical Oceanography*, *48*(7), 1495–1511. https://doi.org/10.1175/JPO-D-18-0015.1

Klenz, T., Simmons, H. L., Centurioni, L., Lilly, J. M., Early, J. J., & Hormann, V. (2022). Estimates of near-inertial wind power input using novel in situ wind measurements from MiniMet surface drifters in the Iceland Basin. *Journal of Physical Oceanography*, *52*(10), 2417–2430. https://doi.org/10.1175/JPO-D-21-0283.1

Kudryavtsev, V., Golubkin, P., & Chapron, B. (2015). A simplified wave enhancement criterion for moving extreme events. *Journal of Geophysical Research: Oceans*, *120*(11), 7538–7558. https://doi.org/10.1002/2015JC011284

Kudryavtsev, V., Yurovskaya, M., & Chapron, B. (2021). Self-similarity of surface wave developments under tropical cyclones. *Journal of Geophysical Research: Oceans*, *126*(4), e2020JC016916. https://doi.org/10.1029/2020JC016916

Le Hénaff, M., Domingues, R., Halliwell, G., Zhang, J. A., Kim, H.-S., Aristizabal, M., et al. (2021). The role of the Gulf of Mexico Ocean conditions in the intensification of Hurricane Michael (2018). *Journal of Geophysical Research: Oceans*, *126*(5), e2020JC016969. https://doi.org/10.1029/2020JC016969

Lenain, L., & Melville, W. K. (2014). Autonomous surface vehicle measurements of the ocean's response to tropical cyclone Freda. *Journal of Atmospheric and Oceanic Technology*, *31*(10), 2169–2190. https://doi.org/10.1175/JTECH-D-14-00012.1

Longuet-Higgins, M. S., Cartwright, D. E., & Smith, N. D. (1963). Observations of the directional spectrum of sea waves using the motions of a floating buoy. In *Ocean wave spectra* (pp. 111–136). Prentice-Hall.

Montoya, R. D., Osorio Arias, A., Ortiz Royero, J. C., & Ocampo-Torres, F. J. (2013). A wave parameters and directional spectrum analysis for extreme winds. *Ocean Engineering*, *67*, 100–118. https://doi.org/10.1016/j.oceaneng.2013.04.016

Moon, I.-J., Ginis, I., & Hara, T. (2004a). Effect of surface waves on air–sea momentum exchange. Part II: Behavior of drag coefficient under tropical cyclones. *Journal of the Atmospheric Sciences*, *61*(19), 2334–2348. https://doi.org/10.1175/1520-0469(2004)061<2334:EOSWOA>2.0.CO;2

Moon, I.-J., Ginis, I., & Hara, T. (2004b). Effect of surface waves on Charnock coefficient under tropical cyclones. *Geophysical Research Letters*, *31*(20), L20302. https://doi.org/10.1029/2004GL020988

Moon, I.-J., Ginis, I., Hara, T., Tolman, H. L., Wright, C. W., & Walsh, E. J. (2003). Numerical simulation of sea surface directional wave spectra under hurricane wind forcing. *Journal of Physical Oceanography*, *33*(8), 1680–1706. https://doi.org/10.1175/2410.1

Moon, I.-J., Hara, T., Ginis, I., Belcher, S. E., & Tolman, H. L. (2004). Effect of surface waves on air–sea momentum exchange. Part I: Effect of mature and growing seas. *Journal of the Atmospheric Sciences*, *61*(19), 2321–2333. https://doi.org/10.1175/1520-0469(2004)061<2321:EOSWOA>2.0.CO;2

National Hurricane Center. National Hurricane Center | National Oceanic and Atmospheric Administration. United States. (1997). Web archive. Retrieved from https://www.nhc.noaa.gov/archive/recon/2018/REPNT1/

National Oceanic and Atmospheric Administration. (2019). Hurricane Michael upgraded to a Category 5 at time of U.S. Landfall. [Press Release]. Retrieved from https://www.noaa.gov/media-release/hurricane-michael-upgraded-to-category-5-at-time-of-us-landfall

Niiler, P. (2001). The world ocean surface circulation. In G. Siedler, J. Church, & J. Gould (Eds.), *Ocean circulation and climate*, *International geophysics series* (Vol. 77, pp. 193–204). Academic Press.

Oost, W., Komen, G. J., Jacobs, M. J., & Van Oort, C. (2002). New evidence for a relation between wind stress and wave age from measurements during ASGAMAGE. *Boundary-Layer Meteorology*, *103*(3), 409–438. https://doi.org/10.1023/A:1014931624535

PopStefanija, I., Fairall, C. W., & Walsh, E. J. (2021). Mapping of directional ocean wave spectra in hurricanes and other environments. *IEEE Transactions on Geoscience and Remote Sensing*, *59*(11), 9007–9020. https://doi.org/10.1109/TGRS.2020.3042904

Reichl, B. G., Hara, T., & Ginis, I. (2014). Sea state dependence of the wind stress over the ocean under hurricane winds. *Journal of Geophysical Research: Oceans*, *119*(1), 30–51. https://doi.org/10.1002/2013JC009289

Sanabia, E. R., & Jayne, S. R. (2020). Ocean observations under two major hurricanes: Evolution of the response across the storm wakes. *AGU Advances*, *1*(3), e2019AV000161. https://doi.org/10.1029/2019AV000161

Schönau, M., Komaromi, W., Hao, J., Doyle, J., Paluszkiewicz, T., & Centurioni, L. (2024). COAMPS-TC atmospheric data subset for Hurricane Michael [Dataset]. Dryad. https://doi.org/10.5061/dryad.b2rbnzsp5

Smedman, A., Högström, U., Sahleé, E., Drennan, W. M., Kahma, K. K., Pettersson, H., & Zhang, F. (2009). Observational study of marine atmospheric boundary layer characteristics during swell. *Journal of the Atmospheric Sciences*, *66*(9), 2747–2763. https://doi.org/10.1175/2009JAS2952.1

Smith, S. D., Anderson, R. J., Oost, W. A., Kraan, C., Maat, N., DeCosmo, J., et al. (1992). Sea surface wind stress and drag coefficients: The HEXOS results. *Boundary-Layer Meteorology*, *60*(1–2), 109–142. https://doi.org/10.1007/BF00122064

Tamizi, A., Alves, J., & Young, I. R. (2021). The physics of ocean wave evolution within tropical cyclones. *Journal of Physical Oceanography*, *51*, 2373–2388. https://doi.org/10.1175/JPO-D-21-0005.1

Tamizi, A., & Young, I. R. (2020). The spatial distribution of ocean waves in tropical cyclones. *Journal of Physical Oceanography*, *50*(8), 2123–2139. https://doi.org/10.1175/JPO-D-20-0020.1

Thomson, J. (2012). Wave breaking dissipation observed with "SWIFT" drifters. *Journal of Atmospheric Technology*, *29*(12), 1866–1882. https://doi.org/10.1175/JTECH-D-12-00018.1

Toba, Y., Iida, N., Kawamura, H., Ebuchi, N., & Jones, I. S. F. (1990). Wave dependence of sea-surface wind stress. *Journal of Physical Oceanography*, *20*(5), 705–721. https://doi.org/10.1175/1520-0485(1990)020<0705:WDOSSW>2.0.CO;2

Tolman, H. L. (2009). User manual and system documentation of WAVEWATCH III TM version 3.14. Technical Note. *MMAB Contribution*, *276*, 220.

Volkov, Y. (2001). The dependence on wave age. In I. S. F. Jones & Y. Toba (Eds.), *Wind stress over the ocean* (pp. 206–217). Cambridge Univ. Press.

Wadler, J. B., Zhang, J. A., Rogers, R. F., Jaimes, B., & Shay, L. K. (2021). The rapid intensification of Hurricane Michael (2018): Storm structure and the relationship to environmental and air–sea interactions. *Monthly Weather Review*, *149*(1), 245–267. https://doi.org/10.1175/MWR-D-20-0145.1

Wright, C. W., Walsh, E. J., Vandemark, D., Krabill, W. B., Garcia, A. W., Houston, S. H., et al. (2001). Hurricane directional wave spectrum spatial variation in the open ocean. *Journal of Physical Oceanography*, *31*(8), 2472–2488. https://doi.org/10.1175/1520-0485(2001)031<2472:HDWSSV>2.0.CO;2

Young, I. R. (1998). Observations of the spectra of hurricane generated waves. *Ocean Engineering*, *25*(4–5), 261–276. https://doi.org/10.1016/S0029-8018(97)00011-5

Young, I. R. (2003). A review of the sea state generated by hurricanes. *Marine Structures*, *16*(3), 201–218. https://doi.org/10.1016/S0951-8339(02)00054-0

Young, I. R. (2006). Directional spectra of hurricane wind waves. *Journal of Geophysical Research*, *111*(C8), C08020. https://doi.org/10.1029/2006JC003540

Zhang, J. A., & Uhlhorn, E. W. (2012). Hurricane sea surface inflow angle and an observation-based parametric model. *Monthly Weather Review*, *140*(11), 3587–3605. https://doi.org/10.1175/MWR-D-11-00339.1

Zhao, B., Wang, G., Zhang, J. A., Liu, L., Liu, J., Xu, J., et al. (2022). The effects of ocean surface waves on tropical cyclone intensity: Numerical simulations using a regional atmosphere-ocean-wave coupled model. *Journal of Geophysical Research: Oceans*, *127*(11), e2022JC019015. https://doi.org/10.1029/2022JC019015

Zhou, X., Hara, T., Ginis, I., D'Asaro, E., Hsu, J., & Reichl, B. G. (2022). Drag coefficient and its sea state dependence under tropical cyclones. *Journal of Physical Oceanography*, *52*(7), 1447–1470. https://doi.org/10.1175/JPO-D-21-0246.1